WEST VIRGINIA UNIVERSITY

PLASMA PHYSICS GROUP

INTERNAL REPORT

Study of the Different Line Broadening Mechanisms for the Laser Induced Fluorescence Diagnostic of the HELIX and LEIA Plasmas.

R.F. Boivin

July 1998
(Revised December 2000)

A-Linewidth

General Definition

Spectral lines in discrete absorption or emission spectra are never strictly monochromatic. One observed a spectral distribution I (λ) of the absorbed or emitted intensity around the central wavelength given by:

$$\lambda_o = h\, c\, (E_i - E_k)^{-1} \qquad (A.1)$$

where λ_o corresponds to an atomic (or molecular) transition with the energy difference between upper and lower level given by $\Delta E = E_i - E_k$. The function $I(\lambda)$ in the vicinity of λ_o is called the line profile (see Fig. A.1). The wavelength interval $\Delta\lambda = |\lambda_2 - \lambda_1|$ between the 2 wavelength λ_2 and λ_1 for which $I(\lambda_1) = I(\lambda_2) = I(\lambda_o)/2$ is the full width at half maximum of the line (FWHM). It is also called the linewidth of the spectral line. The linewidth is sometimes written in terms of frequency ν (or even in terms of angular frequency $\omega = 2\pi\nu$). From $\lambda = c / \nu$, it follows that:

$$\Delta\lambda = c\, \Delta\nu / \nu^2 \qquad \text{or} \qquad \Delta\nu = c\, \Delta\lambda / \lambda^2 \qquad (A.2)$$

The relative linewidth, however remains the same in all schemes, namely:

$$|\Delta\lambda / \lambda| = |\Delta\nu / \nu| = |\Delta\omega / \omega| \qquad (A.3)$$

The spectral region within the linewidth is called the kernel of the line while the regions outside ($\lambda < \lambda_1$ and $\lambda > \lambda_2$) are the line wings.

Broadening of the lineshape

The broadening of spectral lines is a complicated function of the environment of the radiating atoms and ions. In the following sections (B to G) we will define and evaluate the different broadening mechanisms present in our experimental setup. The different broadening mechanisms can be identified as follow:

Natural broadening
Doppler broadening
Pressure (Stark) broadening
Zeeman broadening
Power (saturation) broadening
Instrumental broadening

These line-broadening processes are evaluated for the specific LIF system used to probe the HELIX (and LEIA) plasma. A comparison of the different broadening to determine the dominating process or processes is presented in the last section of the document.

Fig. A.1. Line shape

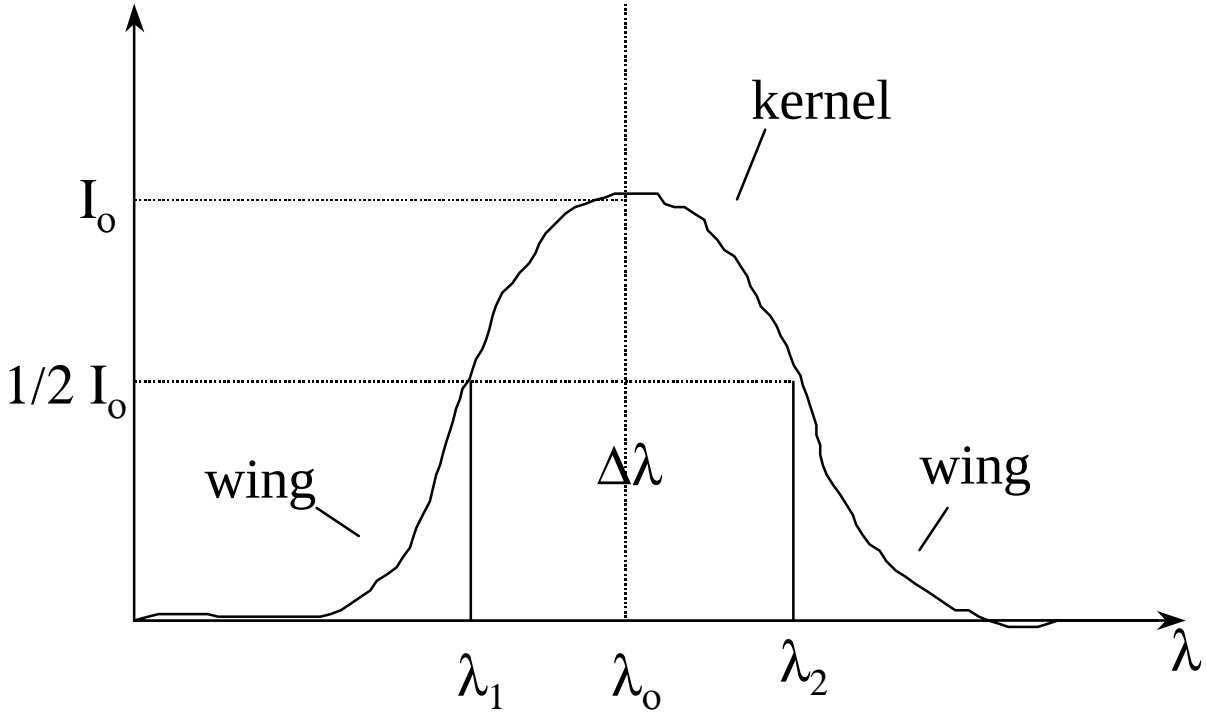

$\Delta\lambda$ = Full Width Half Maximum (FWHM)

B-Natural Linewidth

Theory

The Heisenberg uncertainty principle can be used to evaluate the natural linewidth of a transition between a lower and upper level. Let us consider the mean lifetime τ_i of an excited level E_i with its energy determined with an uncertainty given by:

$$\Delta E_i = (2\pi)^{-1} h / \tau_i \qquad \text{(B.1)}$$

If the lower level E_k is not the ground state but also an excited state with a lifetime τ_k, the uncertainties ΔE_i and ΔE_k of the two levels both contribute to the linewidth yielding the total uncertainty:

$$\Delta E = \Delta E_i + \Delta E_k \qquad \text{(B.2)}$$

in terms of angular frequency, the total uncertainty for this 2 level system is given by:

$$\Delta\omega_{ik} = (\tau_i^{-1} + \tau_k^{-1}) = A_i + A_k \qquad \text{(B.3)}$$

where A_i and A_k are the spontaneous transition probabilities (Einstein coefficients). Thus the total halfwidth of the line is the sum of the width of the upper and lower levels. In the cases where more transitions are possible, the halfwidth is given by the sum of the spontaneous transition probabilities of all lines originating from the two levels. Thus, the natural halfwidth is in general for a line arising between state i and k given by the expression:

$$\Delta\omega_{ik} = \sum_m A_{mi} + \sum_n A_{nk} \qquad \text{(B.4)}$$

Calculated halfwidth

Let us consider the absorption line of our LIF system. The transition is given by:

$$\text{Ar II (3d' } {}^2G_{9/2} \text{)} + hc / \lambda_{6115Å} \rightarrow \text{Ar II (4p' } {}^2F^0_{7/2} \text{)} \qquad \text{(B.5)}$$

where the 3d' $^2G_{9/2}$ level is according to Ar II Grotrian diagram (and the atomic energy level tables) a metastable state. This implies that all transitions originating from this level have very small spontaneous transition probability when compare to the transition originating from the 4p' $^2F^0_{7/2}$ level. This lead to the condition:

$$\sum_m A_{mi} >>> \sum_n A_{nk} \qquad \text{(B.6)}$$

equation (B.4) becomes:

$$\Delta\omega_{ik} \cong \sum_m A_{mi} \qquad \text{(B.7)}$$

Thus, the natural halfwidth in our case is only the sum of the spontaneous transition probabilities of all lines originating from the upper excited level. From the excited upper level 4p' $^2F^0_{7/2}$ we have the following transitions:

Transition	Wavelength (Å)	A (x 10^6 s^{-1})
Doublet-Doublet terms:		
1- 4p' $^2F^0_{7/2}$ ➔ 4S' $^2D_{5/2}$	4610 *	75.9
2- 4p' $^2F^0_{7/2}$ ➔ 3d $^2F_{7/2}$	4682	0.8
3- 4p' $^2F^0_{7/2}$ ➔ 3d' $^2G_{9/2}$	6115 **	21.2
4- 4p' $^2F^0_{7/2}$ ➔ 3d' $^2G_{7/2}$	6123	0.9
5- 4p' $^2F^0_{7/2}$ ➔ 3d $^2D_{5/2}$	5141	8.4
6- 4p' $^2F^0_{7/2}$ ➔ 3d $^2F_{5/2}$	4905	4.1
Doublet-Quadruplet terms:		
7- 4p' $^2F^0_{7/2}$ ➔ 3d $^4D_{7/2}$	2617	0.03
8- 4p' $^2F^0_{7/2}$ ➔ 3d $^4D_{5/2}$	2627	0.02
9- 4p' $^2F^0_{7/2}$ ➔ 3d $^4P_{5/2}$	4413	6.0
10- 4p' $^2F^0_{7/2}$ ➔ 3S $^4P_{5/2}$	2754	0.2
	Total:	117.56

* Fluorescence line
** Pump line

The natural halfwidth for our absorption line is:

$$\Delta\omega_{ik} \cong 1.18 \times 10^6 \text{ s-1}$$
$$\Delta\nu_{ik} \cong 18.7 \text{ MHz}$$
$$\Delta\lambda_N = \Delta\lambda_{ik} \cong 2.33 \times 10^{-4} \text{ Å}$$

References:

A. Corney, Atomic and Laser Spectroscopy, Clarendon Press (1977)
W. Demtröder, Laser Spectroscopy, Spinger Verlag (1981)
G. Garcia and J. Campos J. Quant. Spectrosc. Radiat. Transfer **34**, 85 (1985)
P. Varga, W. Hofer and H Winter J. PhysB:At Mol. Phys. **14**, 1341 (1981)
B.F.J. Luyken Physica **60**, 432, (1972)
G. Norlén, Physica Scripta **8**, 249, (1973)
S. Bashkin and J.O. Stoner, Atomic Energy Levels and Grotrian Diagrams, N. Holland (1975)
W.L. Wiese, M.W. Smith, B.M. Glennon Atomic Transition Probabilities, NSRDS-NBS (1966)
C.H. Moore, Atomic Energy Levels NSRDS-NBS (1971)

FIG. B.1.

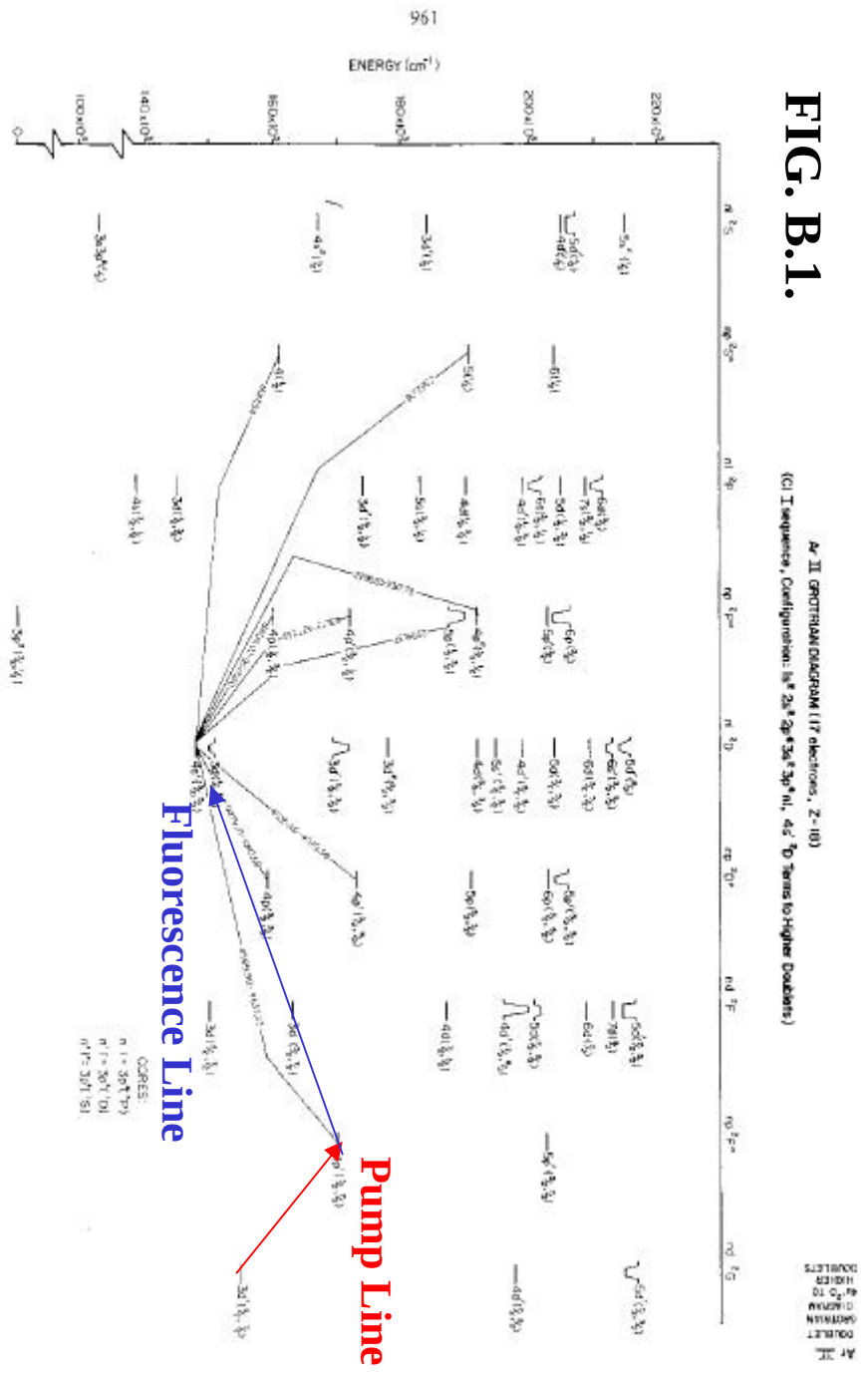

C-Doppler Broadening

Theory

The motion of a radiating particle toward or away from an observer leads to a frequency shift of the emitted line, the Doppler shift. In plasmas, the random motions of the radiating particles cause a Doppler broadening of the lines. If the velocity component of a radiating particle is parallel to the direction of observation, then the frequency appears to be shifted due to the Doppler effect by the amount:

$$\Delta\nu = \nu - \nu_o = \pm \nu_o \, v / c \qquad \text{(C.1)}$$

where v is the particle velocity component in the line of sight and ν_o is the unshifted frequency. With the assumption that the motion of the plasma particles is of a purely thermal nature, one obtains a Maxwellian velocity distribution for the emitters. The line shape can be written as:

$$I(\nu) = I(\nu_o) \exp\left[-(\nu - \nu_o)^2 c^2 \, v_{th}^{-2} \, \nu_o^{-2}\right] \qquad \text{(C.2)}$$

where $v_{th} = (2kT/m)^{1/2}$ is the most probable velocity of the particle distribution. Using equation (C.1) and defining $\sigma^2 = c^{-2} \, v_{th}^{2} \, \nu_o^{2}$; equation (C.2) can be written as:

$$I(\nu) = I(\nu_o) \exp\left[-\Delta\nu^2/\sigma^2\right] \qquad \text{(C.3)}$$

the halfwidth at half maximum is obtain when the exponential term is equal to ½. This corresponds to:

$$\Delta\nu = (\ln 2)^{1/2} \, \sigma = (\ln 2)^{1/2} \, v_{th} \, \nu_o / c \qquad \text{(C.4)}$$

Re-writing equation (C.4) in terms of the particle temperature, the full width half maximum (FWHM) of the line shape is:

$$\Delta\nu_{1/2} = (8 \ln 2 \, kT \, \nu_o^{2} \, m^{-1} \, c^{-2})^{1/2} \qquad \text{(C.5a)}$$

or

$$\Delta\lambda_{1/2} = (8 \ln 2 \, kT \, \lambda_o^{2} \, m^{-1} \, c^{-2})^{1/2} \qquad \text{(C.5b)}$$

Calculated Doppler Broadening

We need to calculate the Doppler Broadening for the following transition:

$$\text{Ar II } (3d' \, {}^2G_{9/2}) + hc / \lambda_{6115Å} \rightarrow \text{Ar II } (4p' \, {}^2F^0_{7/2}) \qquad \text{(C.6)}$$

Replacing the different numerical values the Doppler broadening for this transition in equation (C.5b) we obtain:

$$\Delta\lambda_{d1/2} \, (Å) = 7.46 \times 10^{-2} \, (T)^{1/2} \qquad \text{(with T in eV)} \qquad \text{(C.7)}$$

Using the latest expression, the Doppler Broadening is calculated for a number of ion temperatures. The calculated values are shown in table C.1 and in Fig C.1.

Table C.1

Doppler Broadening of the Ar II (6115 Å) transition at different ion temperature

Ion Temperature (eV)	**$\Delta\lambda_{d1/2}$ (Å)**
.001	2.36×10^{-3}
.005	5.28×10^{-3}
.010	7.46×10^{-3}
.050	1.67×10^{-2}
.100	2.36×10^{-2}
.500	5.28×10^{-2}
1.00	7.46×10^{-2}
5.00	1.67×10^{-1}
10.00	2.36×10^{-1}

References:

A. Corney, Atomic and Laser Spectroscopy, Clarendon Press (1977)
W. Demtröder, Laser Spectroscopy, Spinger Verlag (1981)
W.L. Wiese in Plasma Diagnostic Techniques (chap. 6) R.H. Huddlestone and S. Leonard Academic Press (1965)

Fig. C.1 Doppler Broadening for the Ar II (6115 A) transition as a function of ion temperature

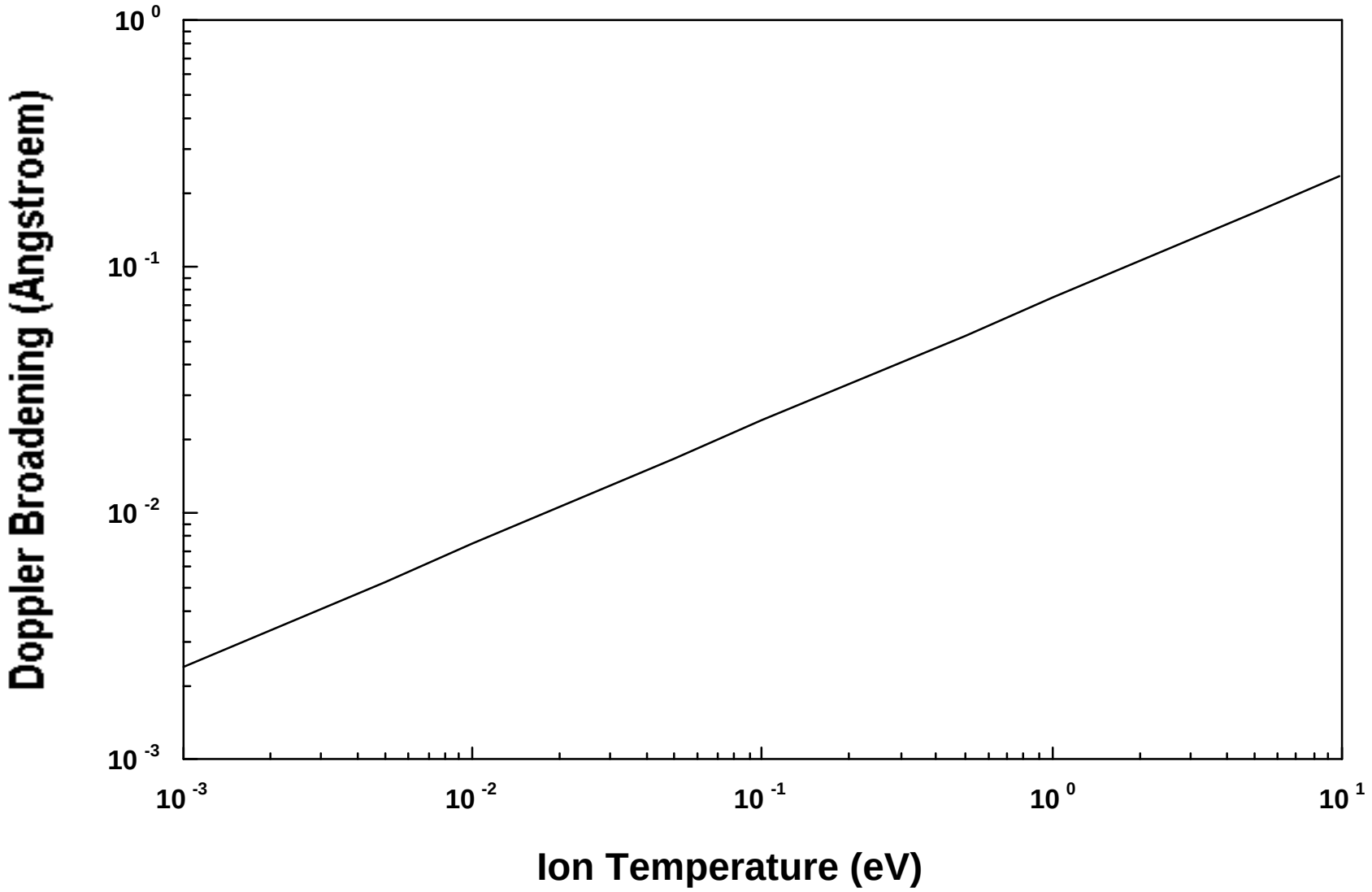

D-Pressure Broadening or Stark Broadening

Theory

Pressure broadening includes the effects of collisions with neutrals particles (Van der Waals broadening), resonance interactions between identical particles (resonance broadening), and collisions with charged particles (Stark Broadening). The first two mechanism are important in a weekly ionized plasma while the last is most important for a highly ionized plasma. For a highly ionized, high density plasma, strong electric field resulting from charged particles produce a broadening of the transitions between the split atomic levels. The broadening associated with these micro electric fields is essentially the Stark broadening. Since these electric fields are random in magnitude and direction, the observed spectral lines appear broadened rather than as distinct lines.
The full width at half maximum associated with the Stark effect $\Delta\lambda s_{1/2}$ (in Å), and the Stark effect shift $\Delta\lambda_S$ are given by the expressions [Griem]:

$$\Delta\lambda s_{1/2} \approx 2 \times 10^{-16}\, \omega\, N_e [1 + 1.75 \times 10^{-4}\, N_e^{1/4}\, \alpha \{1 - 1.02 \times 10^{-3}\, N_e^{1/6}\, T_e^{-1/2}\}] \qquad (D.1)$$

$$\Delta\lambda s \approx 10^{-16}\, \omega\, N_e [(d/\omega) + 2.0 \times 10^{-4}\, N_e^{1/4}\, \alpha \{1 - 1.02 \times 10^{-3}\, N_e^{1/6}\, T_e^{-1/2}\}] \qquad (D.2)$$

where ω is the electron impact half width parameter, α the ion broadening parameter, d is the electron impact shift parameter, N_e is the electron density (cm^{-3}) and, T_e is the electron temperature (eV), respectively. The first 3 parameter are tabulated for a number of Ar ion transitions as a function of electron temperature in ref [Griem]. Equations (D.1) and (D.2) are sufficiently accurate, providing the following conditions are fulfilled:

$$10^{-4}\, \alpha\, N_e^{1/4} < 0.5 \qquad (D.3a)$$

$$8.4 \times 10^{-4}\, T_e^{-1/2}\, N_e^{1/6} < 0.8 \qquad (D.3b)$$

Replacing values relevant to our plasma ($T_e \approx 5$ eV) these conditions can be rewritten solely in terms of electron density:

$$N_e < 1 \times 10^{20}\ cm^{-3} \qquad (D.4)$$

which easily covers all of our operating range. Note that equation (D.1) and (D.2) are better suited to predict Stark broadening and Stark shift at high plasma density ($N_e > 10^{15}$ cm^{-3}) since the small broadening/shift at low density is often smaller than the uncertainty associated with equations (D.1) and (D.2) [Wiese].

Calculated Stark broadening and Stark shift

Let us consider the absorption line of our LIF system as described by:

$$\text{Ar II } (3d'\ ^2G_{9/2}) + hc/\lambda_{6115Å} \rightarrow \text{Ar II } (4p'\ ^2F^0_{7/2}) \qquad (D.5)$$

Unfortunately this transition isn't part of the list of Ar II transitions for which the α and ω parameters have been tabulated [Griem] . We choose instead to average out all parameters over the 22 transitions listed and the mean parameters are shown in Fig. D.1 and Fig. D.2 as a function of electron temperature. Parameter values at electron temperature of 1, 5, and 10 eV are obtained by both interpolation and extrapolation of existing values. Using equation (D.1), Stark broadening is calculated for these 3 electron temperatures and shown in Fig. D.3 as a function of electron density. For a plasma with electron temperature of 5 eV and a electron density of 1×10^{13} cm^{-3} the Stark broadening is:

$$\Delta\lambda_{s1/2} = 1.16 \times 10^{-5} \text{ Å}$$

A similar problem rises when we want to evaluate the Stark shift. The electron impact shift parameter for the specific transition is unknown. We can obtain an approximative value (within an order of magnitude) by using a relative electron impact shift parameter (d/ω) equal to unity ($\approx$ the average value of d/ω for all 22 transitions listed). The ion Stark shifts are usually negative (blue shifted). Using equation (D.2) with $d/\omega \approx 1$ we calculated the Stark shift for 3 different electron temperatures (1,5 and 10 eV). These shifts are shown in Fig. D.4 as function of plasma density. For plasmas with electron temperature of 5 eV and a electron density of 1×10^{13} cm^{-3} the Stark shift is:

$$\Delta\lambda_{s} = 5.8 \times 10^{-6} \text{ Å}$$

References:

W.L. Wiese in Plasma Diagnostic Techniques (chap. 6) R.H. Huddlestone and S. Leonard Academic Press (1965)
H.R. Griem Plasma Spectroscopy, McGraw-Hill (1964)
H.R. Griem et al. Phys. Rev. **125**, 177 (1962)
H.R. Griem, Phys. Rev. **128**, 515 (1962)
M. Baranger, in Atomic and Molecular Processes (chap 13) D.R. Bates, Academic Press (1962)
A. Corney, Atomic and Laser Spectroscopy, Clarendon Press (1977)

Fig. D.1. Alpha parameter vs electron temperature

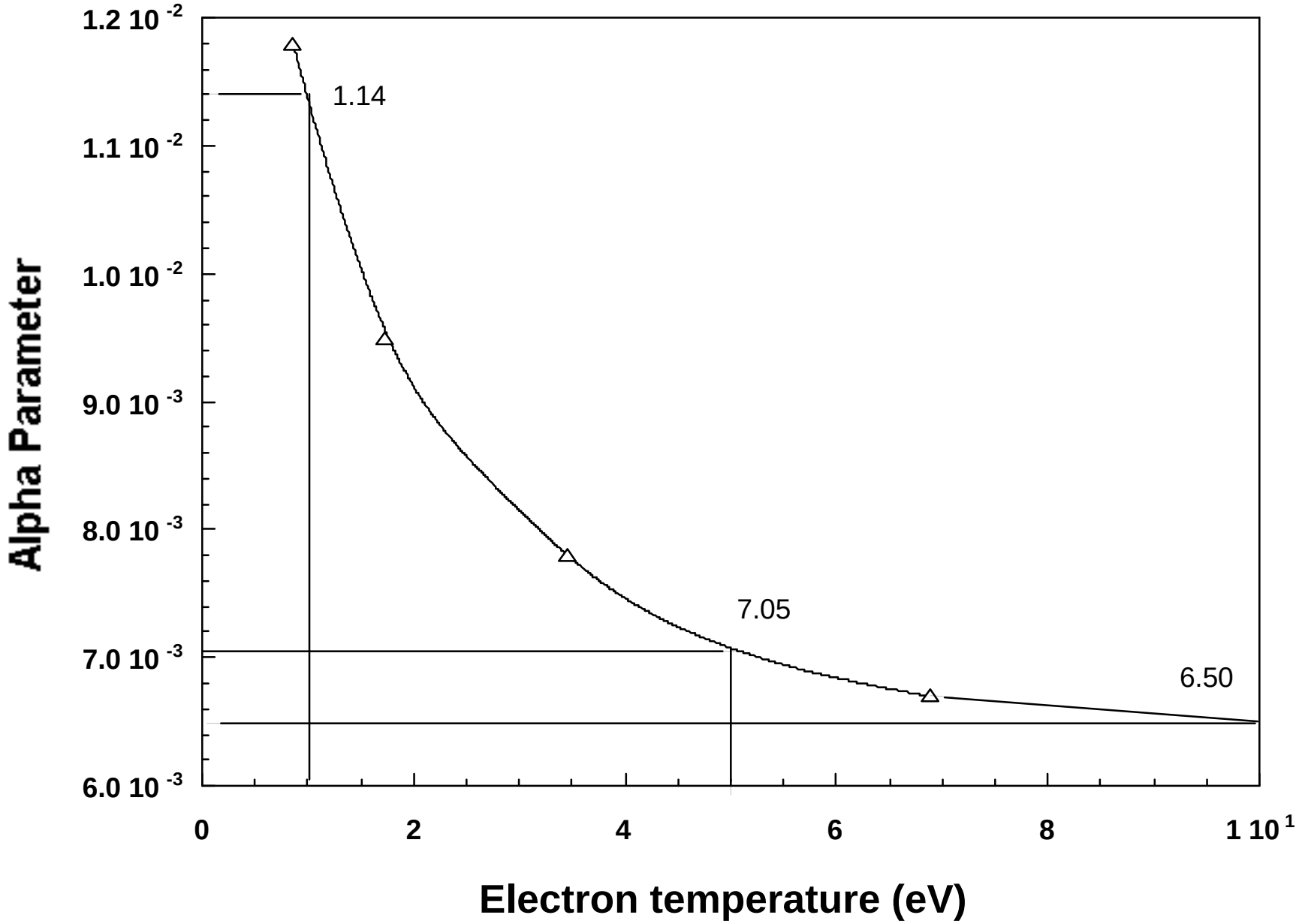

Fig. D.2. W parameter vs electron temperature

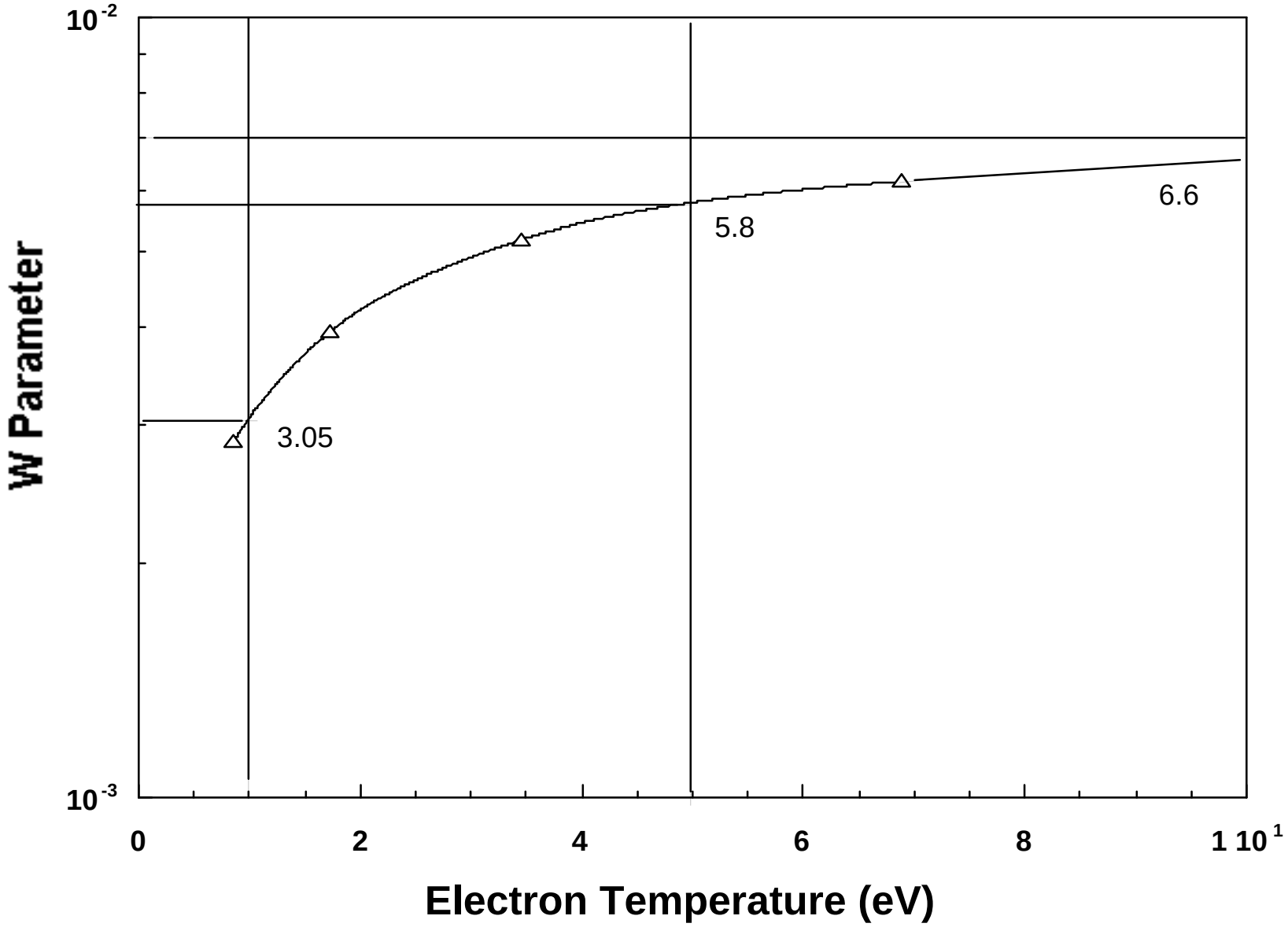

Fig. D.3. Stark broadening as a function of electron density

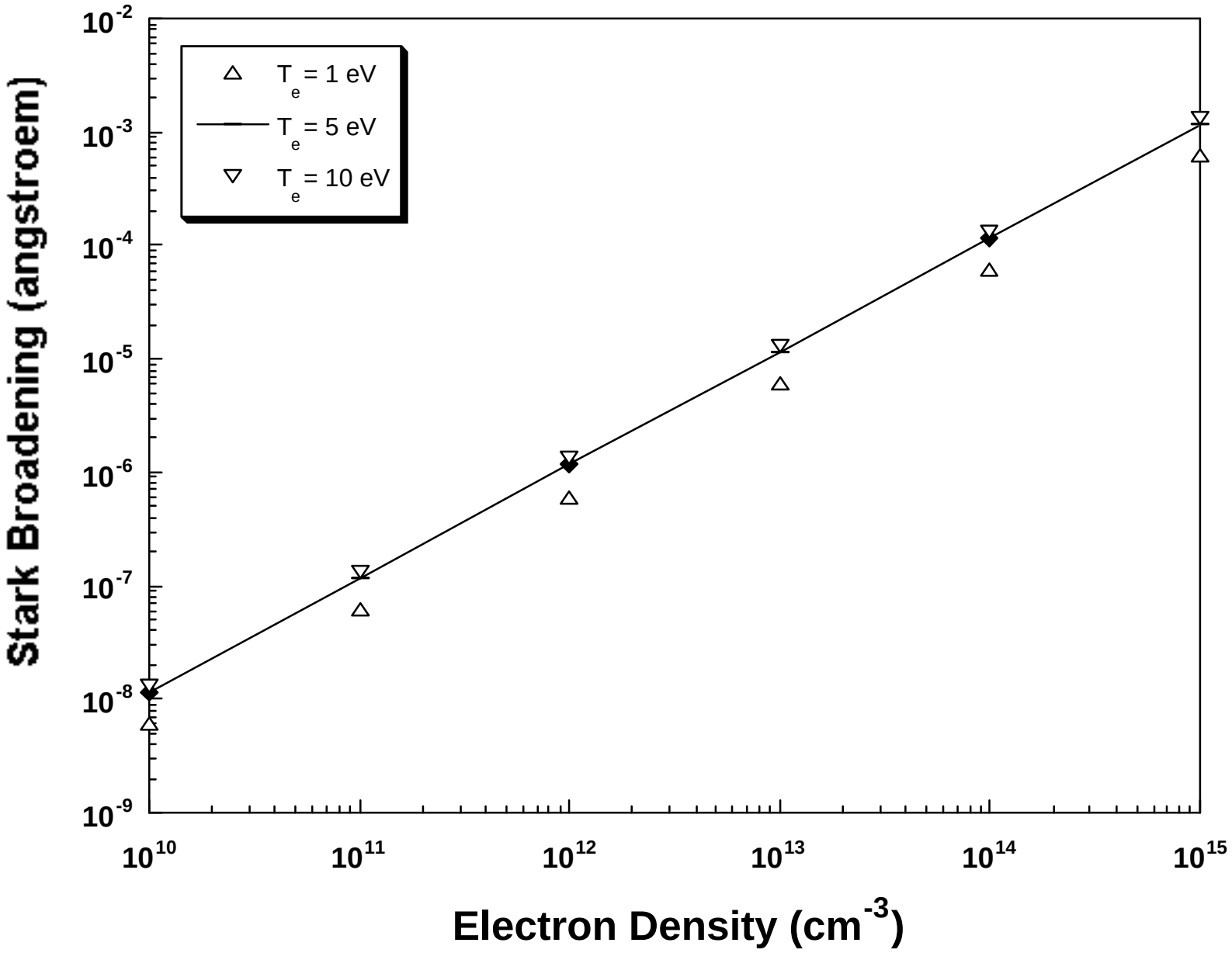

Fig. D.4. Stark shift as a function of plasma density

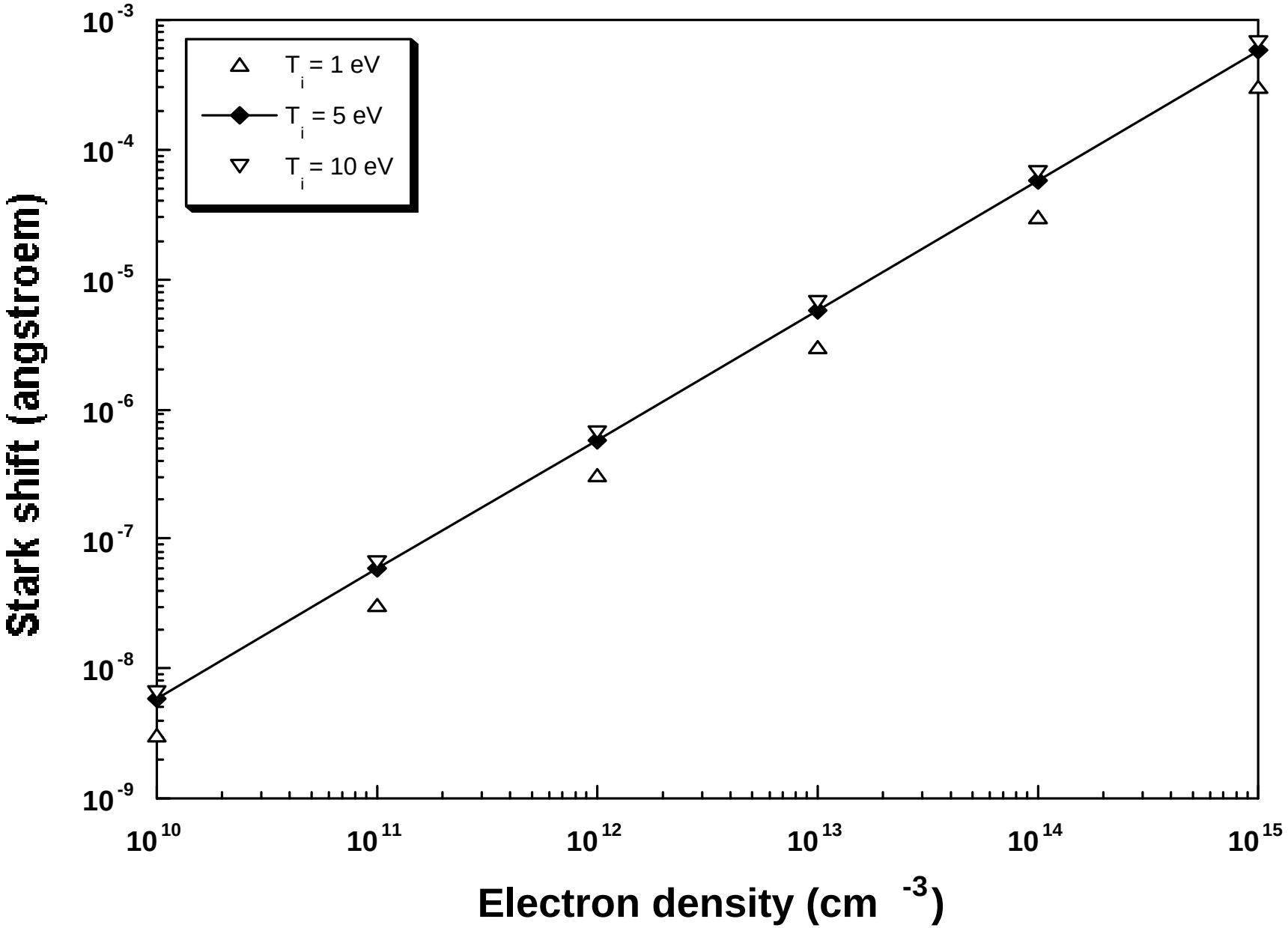

E-Zeeman Broadening

Theory

The interaction of the magnetic moment of an atom with an applied magnetic field results in the splitting of the observed spectral lines. For all lines that are not singlet, the so-called anomalous Zeeman effect is observed. It consists of a splitting into many components with separations that are rational multiples of the normal splitting. The number of energy levels obtained in a magnetic field depends upon the total angular momentum value and is given by (2J +1) (see Fig. E.1). The energy difference introduced by the interaction of magnetic moment and magnetic field B is given by [Marr]:

$$\Delta E = e\, h\, (4\pi m_e)^{-1}\, B\, g_j\, M_j = \beta\, B\, g_j\, M_j \qquad \text{(E.1)}$$

where $\beta = eh / (4\pi m_e) = 9.274 \times 10^{-24}$ Joule Tesla^{-1} is the Bohr magneton, M_j is the magnetic orbital quantum number and, g_j is the Landé factor which differ from level to level. The Landé factor depends on the values of the quantum numbers L (orbital angular momentum), S (angular momentum) and J (total angular momentum) and is given by [Herzberg]:

$$g_j = 1 + [\, \{J(J+1) + S(S+1) - L\,(L+1)\} / \; 2J(J+1) \,] \qquad \text{(E.2)}$$

Considering two split levels (level 1 and 2) the energy associated with the different possible transitions is from equation (E.1) given by:

$$\Delta E = \beta\, B\, (g_1 M_1 - g_2 M_2) \qquad \text{(E.3)}$$

The interaction of the magnetic moment with the magnetic field causes all the terms to split into energy levels with the same spacing since the magnetic orbital quantum number M_j changes only by unity and transitions between one state and another are governed by the normal selection rule:

$$\Delta M_j = 0 \text{ or } \pm 1 \qquad \text{(E.4a)}$$

with: $$M_j = J, J-1, J-2 \ldots\ldots -J \qquad \text{(E.4b)}$$

Transitions for $\Delta M_j = 0$ are called the π components, while transitions with $\Delta M_j = \pm 1$ provides the σ components. In weak to moderate magnetic fields, both the π and σ components are arranged symmetrically about the frequency of zero-field position with the π components being generally less displaced than the σ components. Re-writing equation (E.3) in terms of wavelength (or frequency), the different components π ($M_1 = M_2$) and σ ($M_1 - M_2 = \pm 1$) of the transition will be given by:

$$\Delta\lambda = \beta\, \lambda^2\, B\, c^{-1}\, h^{-1}\, (g_1 M_1 - g_2 M_2) \qquad \text{(E.5a)}$$

or $$\Delta\nu = \beta\, B\, h^{-1}\, (g_1 M_1 - g_2 M_2) \qquad \text{(E.5b)}$$

For a 1 kGauss magnetic field and for our LIF pump line (level $3d^2G_{9/2}$ to level $4p^2F^0_{7/2}$), equation (E.5a) can be written as:

$$\Delta\lambda = 1.74 \times 10^{-2}\ \text{Å}\,(g_1M_1 - g_2M_2) \qquad \text{(E.6)}$$

Calculated Zeeman components

Landé fractional factors for both levels of our LIF system are calculated in this section. A description of the possible values of the magnetic orbital number M_j for both level is given in Fig. E.1. For the metastable level, M_j varies between -9/2 and 9/2 (M_j changes by unit values only), while for the excited level, M_j varies between -7/2 and 7/2. An example of both π and σ transitions is also shown in Fig. E.1. According to the Ar II Grotrian diagram [Bashkin], these are the possible values for the quantum number L, S, J for the 2 levels [Herzberg]:

L = 4 for $3d^2G_{9/2}$ (G-term; doublet),
L = 3 for $4p^2F^0_{7/2}$ (F-term; doublet),
S = 1/2 (doublet) for both levels,
J = 9/2 for $3d^2G_{9/2}$,
J = 7/2 for $4p^2F^0_{7/2}$
M_j = 9/2, 7/2, 5/2, 3/2 …….-9/2 for $3d^2G_{9/2}$
M_j = 7/2, 5/2, 3/2 ,1/2…….-7/2 for $4p^2F^0_{7/2}$

Using equation (E.2) we obtain the Landé factors for the 2 levels:

$g(3d^2G_{9/2}) = 10/9$
$g(4p^2F^0_{7/2}) = 8/7$

The Zeeman splitting is calculated using equation (E.6) and shown in table E.1 and E.2. From the symmetry of the Zeeman pattern, any Zeeman component needs only to be considered from one side of the Zeeman spectra. For the π transitions, the magnetic orbital quantum number for each levels is the same ($M_j = M_1 = M_2$); the calculated values for a 1 kGauss magnetic field are shown in table E.1. For the σ transitions, the magnetic orbital quantum number for each levels is different ($M_1 - M_2 = \pm 1$); the calculated values (B = 1 kGauss) are shown in table E.2
The intensities of all Zeeman components for a J ➔ J + 1 transition is given by the expressions [Marr]:

$M \rightarrow M$ (π components) $\quad I_\pi = 4K\,(J + M + 1)\,(J - M + 1)$ (E.7a)
$M \rightarrow M \pm 1$ (σ components) $\quad I_\sigma = K\,(J \pm M + 1)\,(J \pm M + 2)$ (E.7b)

where K is constant related to the initial line intensity. The total intensities of all Zeeman components is given by:

$$\Pi = \sum_{M'M''} I_\pi + \sum_{M'M''} I_\sigma \qquad \text{(E.8)}$$

The statistical weight of a given Zeeman component is thus:

$$w = \tfrac{1}{2} I_{\pi} / \Pi \quad \text{or} \quad \tfrac{1}{2} I_{\sigma} / \Pi \qquad \text{(E.9)}$$

The ½factor being related to the symmetry of the Zeeman pattern. The statistical weight for all the π-components are calculated using equation (E.9) and shown in table E.1. In a similar fashion the statistical weight for all the σ-components is calculated and shown in table E.2.

Calculated Zeeman Broadening

π-components

The π components are symmetrically distributed around the central unshifted line. The different components with their relative statistical weight are shown in Fig. E. 2a. The distribution is supposed to be Gaussian and the variance σ^2 is given by:

$$\sigma^2 = \sum_i (\lambda_i - m_\lambda)^2 / n \qquad \text{(E.10)}$$

where λ_i is a Zeeman component wavelength and m_λ is the average wavelength (in this case the central wavelength). The summation takes in account the statistical weight of each Zeeman components. From this variance we can obtain the FWHM given by the expression:

$$\text{FWHM} = \Delta\lambda_{Z\pi} = 2 (2 \ln 2)^{1/2} \sigma \qquad \text{(E.11)}$$

The FWHM is the resulting Zeeman broadening for the π components. In the case of a 1 kGauss magnetic field, the Zeeman broadening associated with the π components is:

$$\Delta\lambda_{Z\pi} = 2.6 \times 10^{-3} \text{ Å}$$

σ-components

For the σ components, the situation is different. Two clusters of line are symmetrically shifted on each side of the central line. The distribution pattern is shown in Fig E.2b. Each cluster is asymmetric with the most intense lines closest to the central wavelength. Although the situation is different from the π components, we will use the same approach to calculate the resulting Zeeman broadening. First, we calculate the average wavelength given by:

$$m_\lambda = \sum_i \lambda_i / n = 1.84 \times 10^{-2} \text{ Å} \qquad \text{(E.12)}$$

which means that the average shift of the σ components is ± 1.84 x 10^{-2} Å with respect to the unshifted central wavelength. We now use equations (E.10) and (E.11) to calculate the FWHM. For a 1 kGauss magnetic field, the Zeeman Broadening associated with the σ components is:

$$\Delta\lambda_{Z\sigma} = 2.2 \times 10^{-3} \text{ Å}$$

Because of the asymmetry of the cluster, we can suppose that the real $\Delta\lambda_\sigma$ is probably a bit larger and we will suppose that:

$$\Delta\lambda_{Z\sigma} \approx \Delta\lambda_{Z\pi} \cong 2.6 \times 10^{-3} \text{ Å}$$

As seen in equation (E.5) the Zeeman Broadening is directly proportional to the magnetic field intensity. Using equation (E.5) and the broadening value calculated above we plotted in Fig E.3 the Zeeman Broadening for the $3d^2G_{9/2}$ to $4p^2F^0_{7/2}$ transition as a function of the magnetic field.

References:

G. Herzberg Atomic Spectra and Atomic Structure, Dover (1945)
G. Marr Plasma Spectroscopy, Elsevier (1968)
H.R. Griem Plasma Spectroscopy, McGraw-Hill (1964)
A. Corney, Atomic and Laser Spectroscopy, Clarendon Press (1977)
S. Bashkin and J.O. Stoner, Atomic Energy Levels and Grotrian Diagrams, N. Holland (1975)

Table E.1

Zeeman splitting for the π transitions ($M = M_1 = M_2$)

M	**$(g_1 - g_2)M$**	**$\Delta\lambda$(Å)**	**w**
7/2	7/63	1.93×10^{-3}	0.0333
5/2	5/63	1.38×10^{-3}	0.0583
3/2	3/63	8.10×10^{-4}	0.0750
1/2	1/63	2.76×10^{-4}	0.0833

+ 4 symmetrical components

Table E.2

Zeeman splitting for the σ transitions ($M1 \neq M2$):

M_1	**M_2**	**$g_1M_1 - g_2M_2$**	**$\Delta\lambda$(Å)**	**w**
9/2	7/2	63/63	1.74×10^{-2}	0.0750
7/2	5/2	65/63	1.79×10^{-2}	0.0583
5/2	3/2	67/63	1.85×10^{-2}	0.0438
3/2	1/2	69/63	1.91×10^{-2}	0.0313
1/2	-1/2	71/63	1.96×10^{-2}	0.0208
-1/2	-3/2	73/63	2.02×10^{-2}	0.0125
-3/2	-5/2	75/63	2.07×10^{-2}	0.0063
-5/2	-7/2	77/73	2.13×10^{-2}	0.0021

+ 8 symmetrical components

Fig. E.1. Zeeman splitting

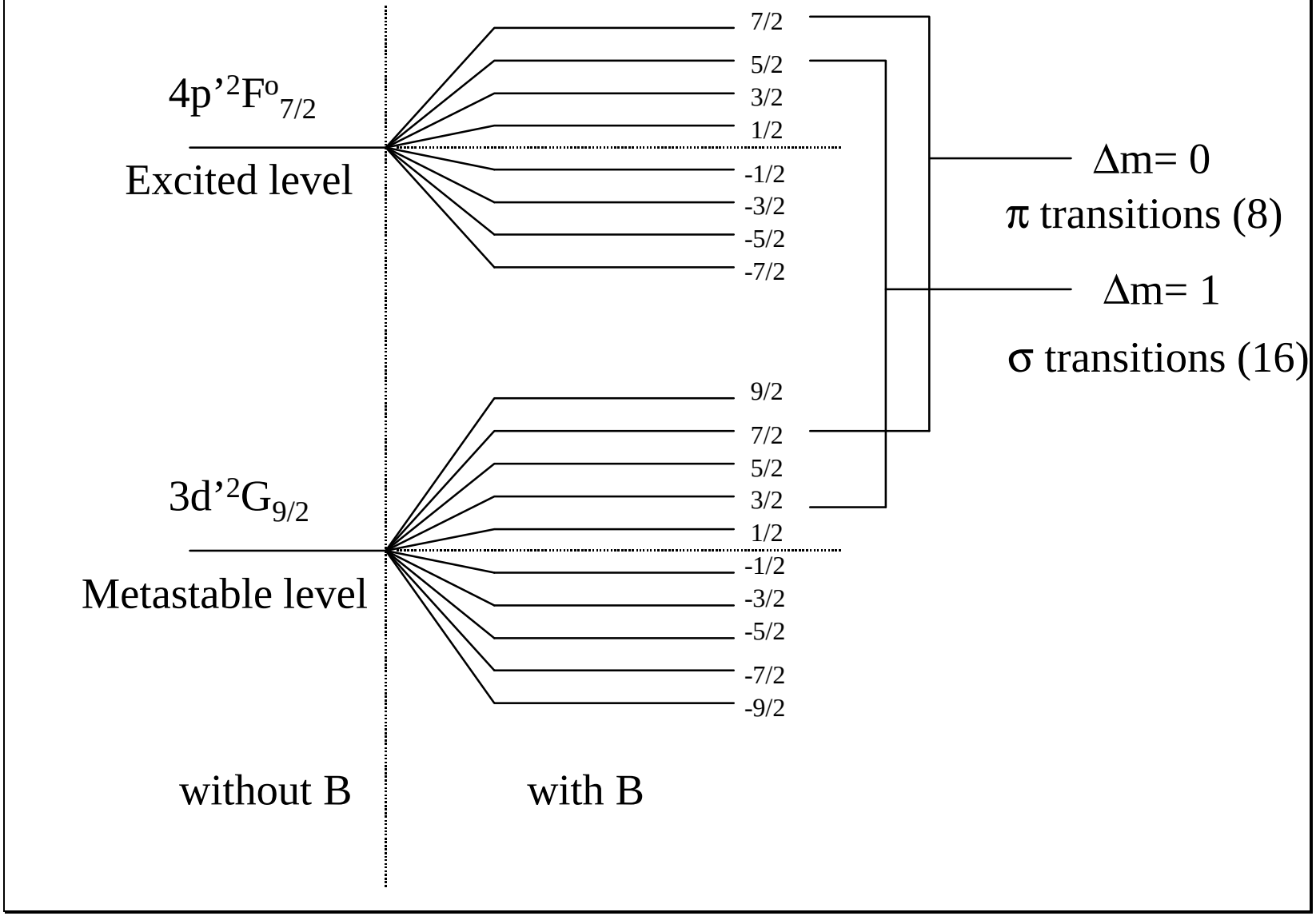

Fig. E.2. Zeeman Splitting

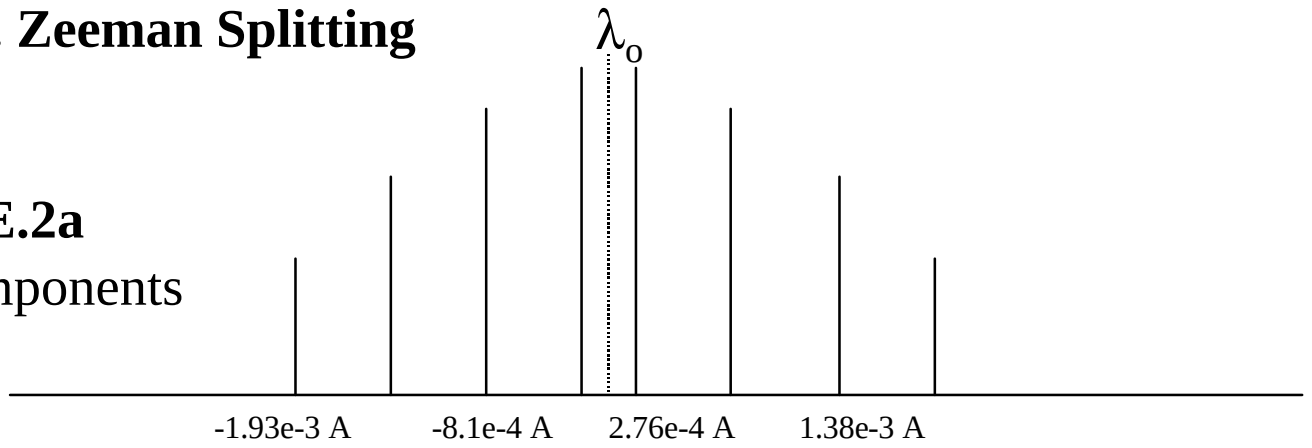

Fig. E.2a

π components

π components

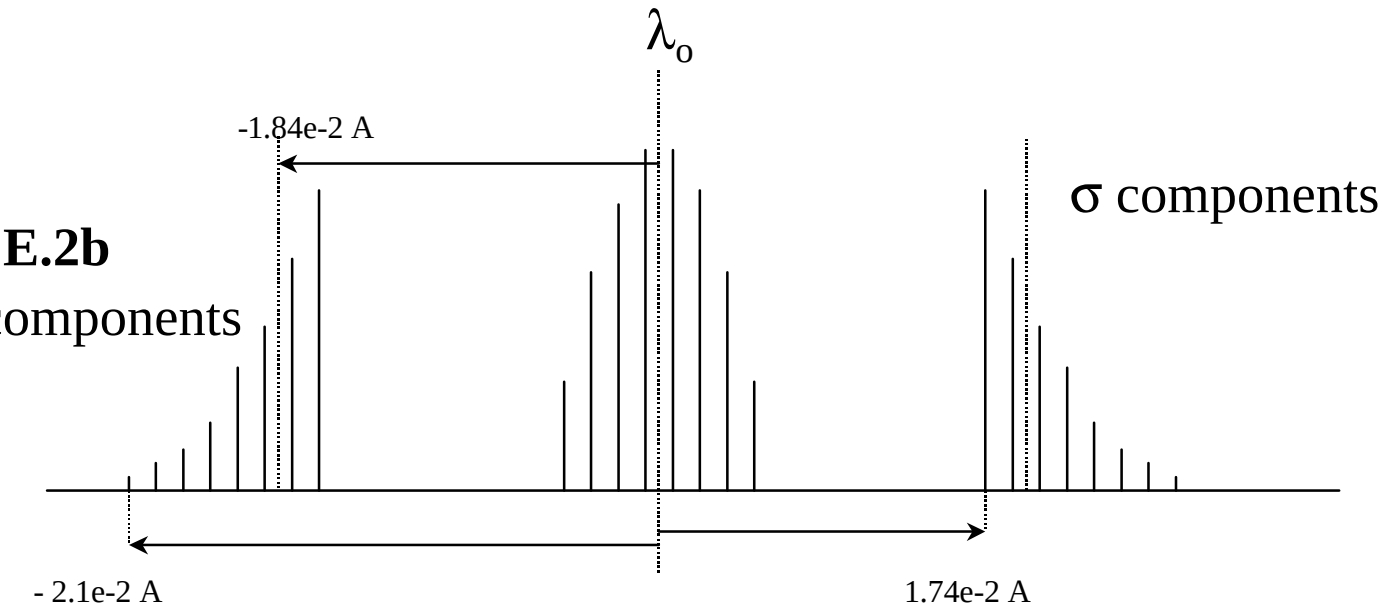

Fig E.2b

$\sigma + \pi$ components

Fig. E.3. Resulting Zeeman Broadening for π and σ transitions as a function of the Magnetic Field Intensity

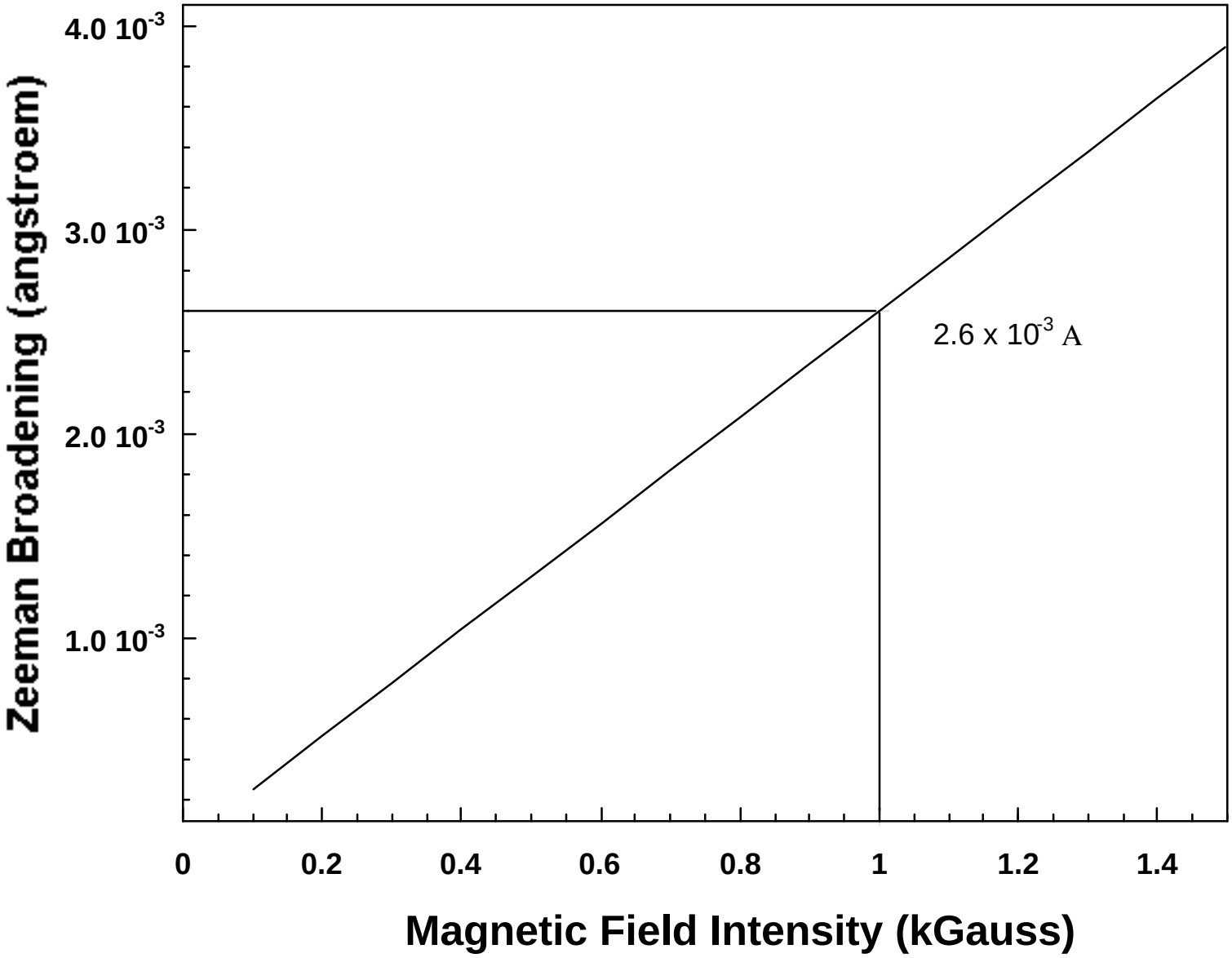

F-Power or saturation broadening

Theory

Power or saturation broadening occurs when the stimulated photon emission rate equals the photon absorption rate and both are greater than the spontaneous emission rate. Further increase in the laser intensity will not change this balance. When saturation occurs, the power residing in the wings of the laser becomes important, resulting in photon absorption far from the laser central line [Demtroeder]. This in turn induces a broadening in the measured fluorescence line, which can be identified as saturation or power broadening. Ignoring power broadening may result in serious measurement errors of the ion temperature. By reducing the laser intensity, this problem can be avoided. However, this scheme can diminish the fluorescence signal below the detection threshold. A balance between a strong signal and a minimal instrumental broadening represents the most desirable situation.

Multiple processes cause power broadening. These processes are absorption, stimulated emission and spontaneous emission of photons. This broadening can only be understood by examining in details how these processes change the population densities of three specific states of an ion involved in the LIF system. Other processes, unrelated to the laser, characterize the population density of the different states of the LIF system. They include ion-ion collisions, electron-ion collisions and spontaneous de-excitation from higher state (cascading de-excitation). Spatial profile of the laser beam is also an important factor that may affect the overall laser broadening.

Thus, for all the reasons mention above, the evaluation of power broadening is no easy task. An extensive set of empirical rate equations governing the LIF process is needed to evaluate the laser broadening effect [Goeckner and Goree]. A complete evaluation of the laser broadening although desirable will not be presented in this document. In its place, a evaluation based on Goeckner and Goree calculation will provide a valid estimation of the effect power broadening on our resulting fluorescence line shape.

Power broadening evaluation

Goeckner and Goree, have studied extensively the effects of power broadening by a 1GHz bandwidth pulsed laser (17 ns) on the following Ar II LIF scheme:

$$3d'\ ^2G_{9/2} + hc / \lambda_{6115Å} \rightarrow 4p'\ ^2F^0_{7/2} \rightarrow 4s'\ ^2D_{5/2} + hc / \lambda_{4610Å} \quad (F.1)$$

which is exactly the same transition that we are using to probe our plasma. Let us consider Fig. F.1., which represents the full width half maximum as a function of ion temperature for different laser power intensities. The uncorrected FWHM curve included in the graph is exclusively associated with the Doppler broadening. For the other discrete values, both Doppler broadening and power broadening are included in the FWHM evaluation. One can see, that for an ion with $T_i \geq 0.1$ eV no significant broadening is observed for a laser intensity less than or equal to 50 kW m^{-2}. For a 1 eV ion, a laser density of the order of 5 MW m^{-2} can be used without inducing power broadening.

In Fig F.2 we have the FWHM as a function of laser intensity for different ion temperature. Again, one can see that for laser density below 50 kW m^{-2} no significant

power broadening can be seen as the different FWHM remain constant as a function of the laser density (the linewidth increase very slightly for the lowest ion temperature). As laser intensity increases, the lower temperature FWHM are the most dramatically affected. Thus, laser broadening will primarily affect low ion temperature measurements and optimization of the laser intensity becomes crucial for these same measurements.

Note that the results presented above are for a laser bandwidth of 1 GHz. Selecting a laser with a narrower bandwidth, which produces less instrumental broadening, lowers the ion temperatures that can be measured accurately. Thus, the discussion presented here represents a worst case scenario since our laser bandwidth is in the MHz range. For our LIF setup, the laser beam has a minimum diameter of 2 mm, with a maximum power of approximately 100 mW. This corresponds to a laser intensity of 38 kW m^{-2}, which produces only a very small amount of broadening as indicated in Fig. F.1 and Fig. F.2. According to Fig. F.1 and F.2 we can estimate roughly the power broadening for a 0.1 eV ion and for a laser density of 38 kW m^{-2} to be:

$$\Delta\lambda_{p1/2} \leq 1 \times 10^{-3} \text{ Å}$$

where the inequality stands for the fact that our laser has a smaller bandwidth than the one used for the calculation. Thus, no significant laser broadening of the resulting fluorescence linewidth is expected for ion with a temperature equal or higher than 0.1 eV. This has been experimentally confirmed by looking at the linewidth while introducing a neutral filter in the laser path to reduce the laser intensity. For lower ion temperatures, the power broadening becomes increasingly important.

An important aspect of this discussion is related to the optimization of the laser intensity for ion temperature measurement. This optimization can be understood by examining Fig. F.3 representing the relative population of the emitting level as a function of laser intensity for different ion temperatures. Saturation broadening occurs when a large fraction of all ions produces fluorescence. The laser power levels can be optimized by determining the asymptotes of the signal strength for high and low intensities. The optimum power densities are obtained by considering the half intensities at which each of these respective asymptotes cross. These optimum power intensities are for the 5 ion temperatures listed in Fig. F.3:

T_i (eV)	**Laser Intensity (W m^{-2})**
0.025	5.0×10^4
0.1	7.5×10^4
0.5	1.5×10^5
1.0	2.5×10^5
5.0	5.0×10^5

These values can be considered the maximum laser power density that can be used to accurately measure a corresponding ion temperature. Laser intensities below the optimum will simply reduce the signal strength for detection. Thus, as suggested in Fig.

F.3, for an ion temperature in the 0.1 to 0.5 eV range our laser intensity could safely be increase by a factor of 2 without inducing any significant laser broadening in the fluorescence linewidth.

References:

W. Demtröder, Laser Spectroscopy, Spinger Verlag (1981)
Goeckner and Goree, J.Vac. Sci. Technol. A **7** (3), 977 (1989)

Fig. F.1. Full width half maximum as a function of ion temperature

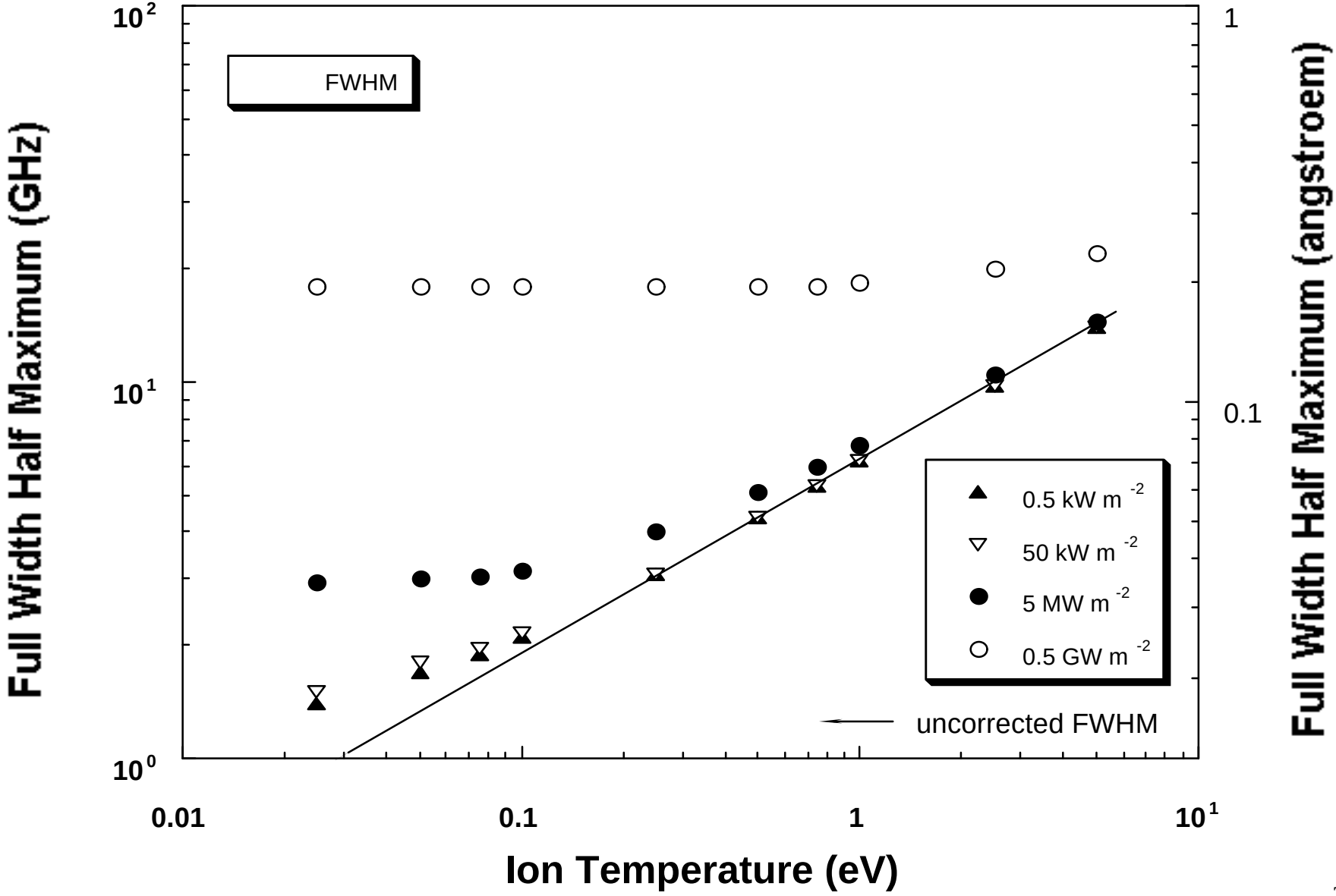

Fig. F.2. Full Width Half Maximum as a function of laser intensity for different ion temperature

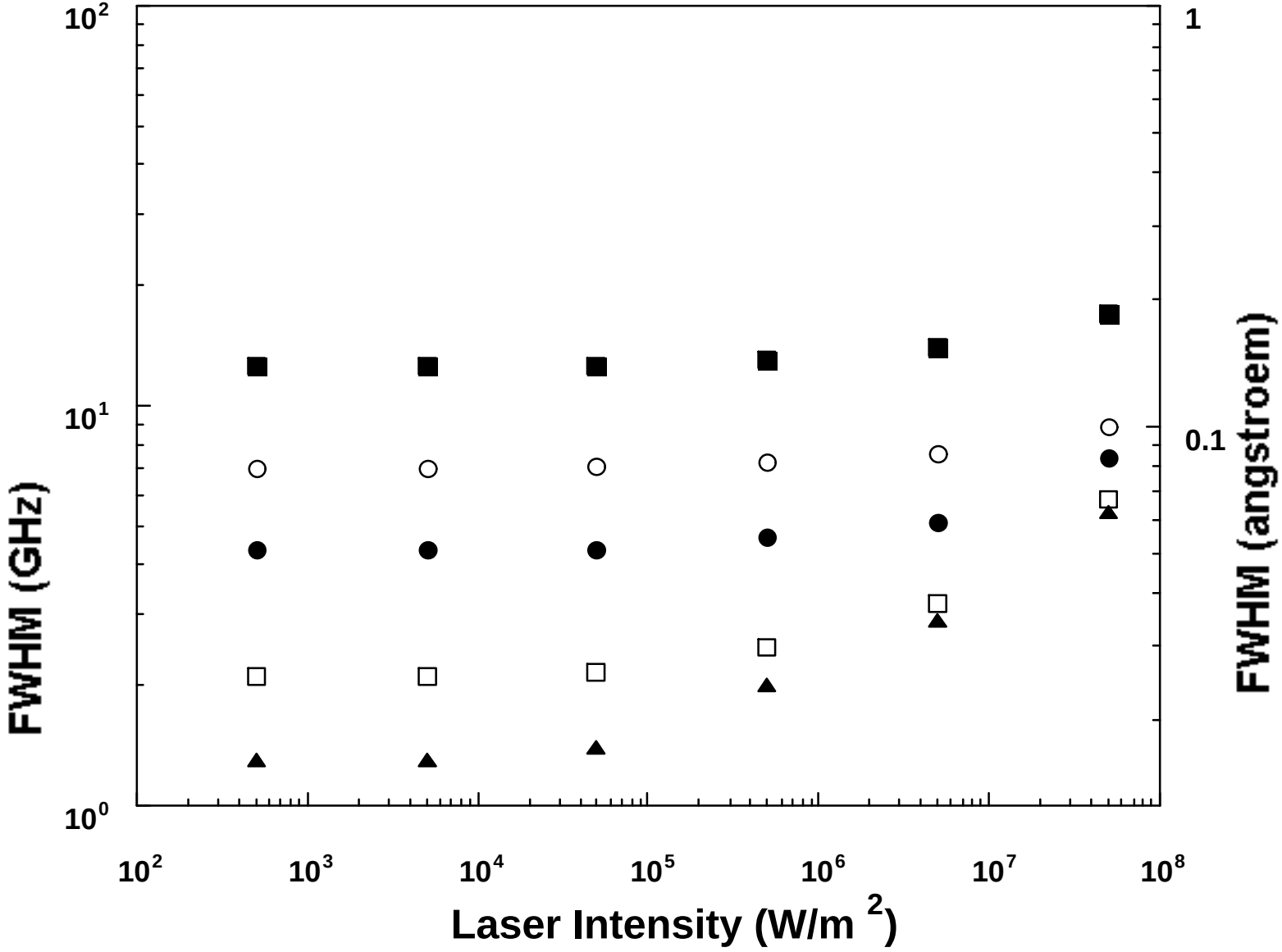

Fig. F.3. Fraction of fluorescent ions as a function of laser intensity

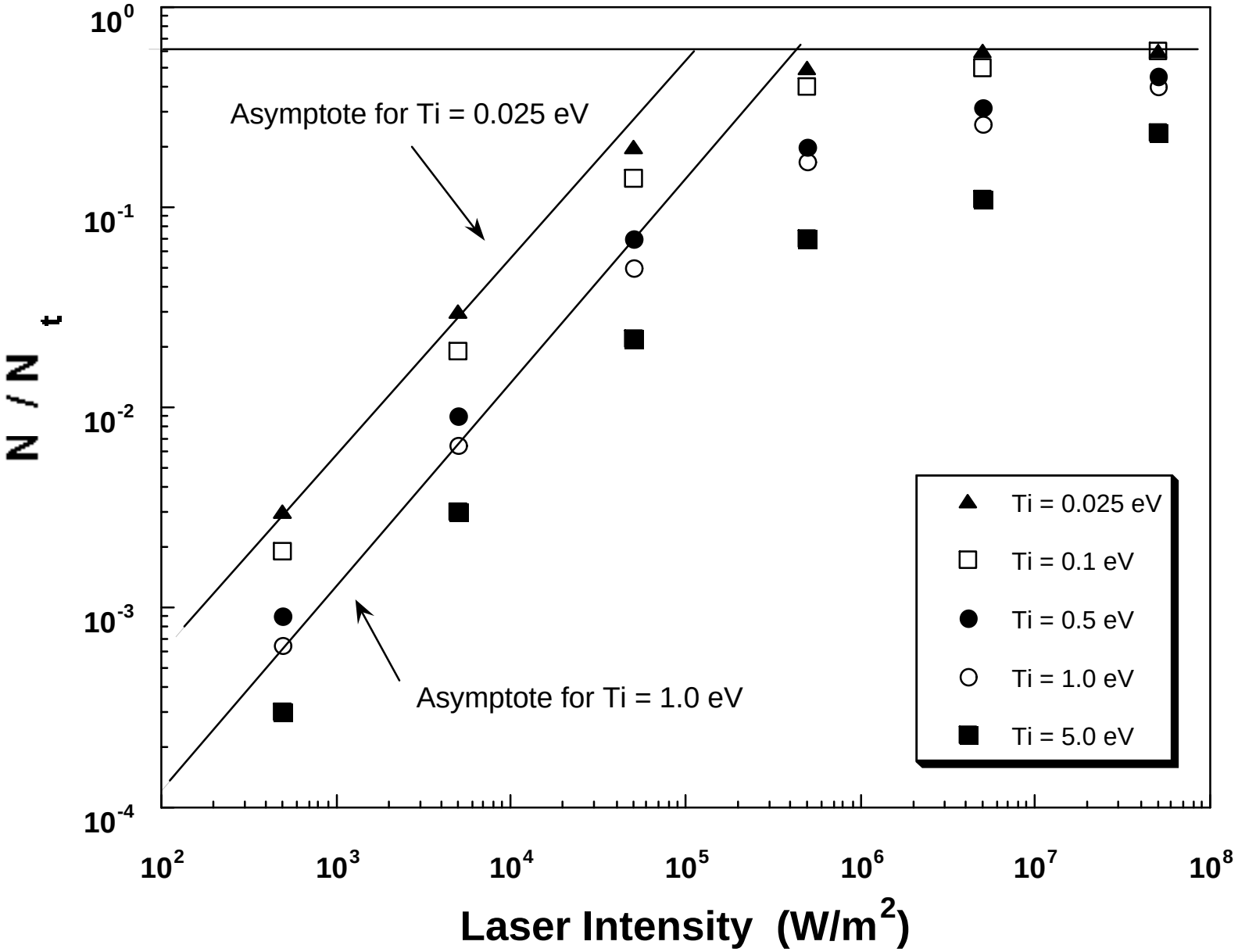

G - Instrumental Broadening

Theory and evaluation

Another broadening mechanism that can affect our measurement of temperature is due to the instrumental broadening. Usually, there are 2 distinct types of instrumental broadening; one is associated with the laser linewidth and the other is related to the dispersion of the light detection system (monochromator). In our experimental setup, since light is directly detected with a passband filter (± 10Å) and a photomultiplier, the second type of instrumental broadening do not applied here.
The finite linewidth of the laser also causes a line broadening in the fluorescence radiation. The laser bandwidth for the Coherent 899 Ring laser is less than 1 MHz:

$$\Delta\lambda_{ins} \leq \ 1.25 \times 10^{-5} \text{ Å}$$

This value is at least 2 order of magnitude less than the Doppler broadening for 0.01 eV ion temperatures.

H - Resulting Broadening

Theory

The resulting lineshape of the broadened fluorescence line is qualitatively important to determine the dominant broadening mechanism(s). A purely Gaussian profile is strongly indicative of Doppler broadening. A distorted or asymmetric Gaussian is indicative of a Zeeman broadening contribution. A Lorentzian profile can either be associated with a natural, Stark, power broadening or a combination of these 3 broadenings. A combination of Doppler and any of the last 3 mentionned broadenings results in a Voigt profile. All of these combinations can be more easily be detected by looking at the wings of the lineshape since the non-Gaussian lineshapes have stronger structure than the Doppler broadening in these wavelength intervals.

Quantitatively, it is important to compare the FWHM of the different possible broadenings and to determine which can be neglected. In most low density (and moderate to high ion temperature) the Doppler broadening is the dominant broadening mechanism with sometimes a secondary non-negligible broadening process. In general, the resulting lineshape from two statistically independent line broadening mechanism with associated lineshapes $I_1(D\lambda_1)$ and $I_2(D\lambda_2)$ is given by the convolution [Griem]:

$$I_{obs}(\Delta\lambda) = \int_{-\infty}^{\infty} I_1(\Delta\lambda - \Delta\lambda')\ I_2(\Delta\lambda')\ d\Delta\lambda' \qquad \text{(H.1)}$$

One can see that if one of the two mechanisms is much smaller than the other (equivalent to replacing $I_2(D\lambda')$ by a delta function) the resulting lineshape is simply the lineshape of the dominant broadening mechanism.

Comparison of the different broadening

Let us consider the different broadening values calculated in this document. The broadening varies according to a wide number of plasma parameter and, we will limit ourselves to the most pertinent plasma conditions. First, let us consider for the following conditions:

Argon plasma
T_i = 0.1 eV,
T_e = 5 eV,
$n_e = 1 \times 10^{13}$ cm^{-3},
B = 1 kGauss,
I_o = 38 kW m^{-2},
λ_o = 6115Å,
$\Delta\nu_{laser}$ = 1 MHz

For these plasma conditions the FWHM for the different broadenings are evaluated and shown in table H.1. A description of the lineshape associated with each broadening is also given in table H.1.

Mechanism	FWHM	Profile type
Natural	$\Delta\lambda_N = 2.33 \times 10^{-4}$ Å	Lorentzian
Doppler	$\Delta\lambda_D = 2.36 \times 10^{-2}$ Å	Gaussian
Stark	$\Delta\lambda_S = 1.16 \times 10^{-5}$ Å	Lorentzian (asymmetric**)
Zeeman	$\Delta\lambda_Z = 2.6 \times 10^{-3}$ Å	Rough Gaussian (π)
	$\Delta\lambda_Z = 2.6 \times 10^{-3}$ Å	Asymmetric (σ components)
Power	$\Delta\lambda_p = 1.0 \times 10^{-3}$ Å	Lorentzian
Instrumental	$\Delta\lambda_Z = 1.25 \times 10^{-5}$ Å	Gaussian ?*

* depends on the spectral distribution of the laser beam
** the ion contribution of the Stark broadening may be asymmetrical [Griem]

under these conditions the Doppler broadening is one order of magnitude greater than any other broadening. The ion temperature can be extracted directly from the fluorescence lineshape (the overestimation in temperature is only 20% in this case). Let us consider the broadening for the maximum magnetic field intensity 1.3 kGauss) and for a low ion temperature (0.05 eV), the Doppler, Zeeman and Power broadenings are:

Doppler	$\Delta\lambda_D$ (0.01 eV) $= 1.67 \times 10^{-2}$ Å
Zeeman	$\Delta\lambda_Z$ (1.3 kGauss) $= 3.4 \times 10^{-3}$ Å
Power	$\Delta\lambda_p$ (0.05 eV) $\approx 1.25 \times 10^{-3}$ Å

Here, one can see that the Zeeman broadening corresponds to about 20% of the Doppler broadening. The resulting FWHM is equivalent to a 0.082 eV ion temperature. Thus, the ion temperature can no longer be directly extracted from the fluorescence lineshape; if so this will lead to an inaccurate ion temperature (overestimation by 64% in this case). Instead, one must use a convolution function similar to equation (H.1). Finally, for an even lower ion temperature (0.01 eV) the situation becomes increasingly worst:

Doppler	$\Delta\lambda_D$ (0.01 eV) $= 7.5 \times 10^{-3}$ Å
Zeeman	$\Delta\lambda_Z$ (1.3 kGauss) $= 3.4 \times 10^{-3}$ Å
Power	$\Delta\lambda_p$ (0.01 eV) $\approx 1.5 \times 10^{-3}$ Å

In this case the Zeeman broadening is about 45% of the Doppler broadening and the total FWHM corresponds to a 0.027 eV ion temperature (170% overestimation). Rule of thumb: a secondary broadening corresponding to 10% or less of the Doppler broadening can be neglected. If not, the convolution equation must be used to obtain the ion temperature.